www.czasopisma.pan.pl PAN POLSKA AKADEMIA NAUK www.journals.pan.pl

Arch. Metall. Mater. **68** (2023), 4, 1563-1570

DOI: https://doi.org/10.24425/amm.2023.146223

MANFENG GONG[1,2], GUANGFA LIU[1,2], MENG LI[1,3*], XIAOQUN XIA[1], LEI WANG[1], JIANFENG WU[1,2], SHANHUA ZHANG[1,2], FANG MEI[1]

BONDING PROPERTIES OF TiAlCrSiN COATING / WC-8Co CEMENTED CARBIDE WITH MICROTEXTURED SURFACE

WC-8Co cemented carbide was prepared by a high-temperature liquid phase sintering in argon at 5-200 Pa. Three microtextured grooves with a spacing of 500, 750, and 1000 μm were prepared on the surface of WC-8Co cemented carbide. TiAlCrSiN multi-element hard coating was deposited on the WC-8Co cemented carbide microtextured surface with multi-arc ion plating technology. The Vickers hardness and fracture toughness of coated and uncoated WC-8Co cemented carbide with or without a microtextured surface were investigated. The effect of different microtextured spacing on the interface bonding strength of the TiAlCrSiN coating was analyzed. The results show that with the reduction of the microtextured spacing, the Vickers hardness of the cemented carbide slightly decreases, and the fracture toughness slightly increases. The microtextured surface can improve the interface bonding strength between the coating and the substrate. The smaller the microtextured spacing, the larger the specific surface area and the higher the surface energy, so the interface bonding strength between the coating and the substrate increases.

Keywords: Cemented carbide; Coating; Microtexture; Mechanical properties; Interface bonding strength

1. Introduction

In recent years, the increasing high-precision processing technology development and the widespread application of difficult processing materials have continuously improved the requirements for the cutting performance of tools. Depositing a coating on the tool's surface can improve its performance [1,2]. The preparation of microtextured in the substrate's surface can reduce the coating's residual stress and improve the residual stress distribution. Meanwhile, it can also enhance the interfacial bonding strength between the substrate and the coating system [3]. Previous reports [4] deposited nickel-phosphorus coating on the microtextured surface. The interfacial bonding strength of the substrate/coating system is characterized by scratches and three-point bending experiments. As a result, the microtextured surface effectively improves the adhesion of coatings. Processing microtexture in the substrate surface by Laser processing technology and depositing the TiAlN coating proves that this method can greatly improve the interfacial bonding properties than the coating of no microtexture [5]. Pit, linear, and bionic sinusoidal textures of the 40Cr alloy steel surface were processed by a laser [6]. Meanwhile, the influence of microtextured surfaces on the bonding mechanism of plasma spraying coating was analyzed through three-dimensional modeling. The linear microtexture and bionic sine microtexture were better at improving the coating quality than the pit microtexture. Having a convex microtexture increased the bonding force of the matrix/coating system. However, most studies concentrate on improving the tool's performance, and there is less research on the influencing factors of the interface bonding strength between the substrate and coating. This article studies the mechanical properties and the interface bonding strength of WC-8Co cemented carbides, with four kinds of microtextured surfaces with different groove spacing.

2. Preparation and experimental method

2.1. Specimen preparation

This experiment selected WC-8Co commercial powder with a particle size of about 2.0 μm as the experimental material. The bulk body of 16.8×16.8×6.0 mm was pressed by an automatic

1 LINGNAN NORMAL UNIVERSITY, SCHOOL OF MECHATRONICS ENGINEERING, ZHANJIANG 524048, CHINA
2 GUANGDONG OCEAN UNIVERSITY, SCHOOL OF MECHANICAL ENGINEERING, ZHANJIANG 524088, CHINA
3 NORTHWESTERN POLYTECHNICAL UNIVERSITY, SCHOOL OF MATERIALS SCIENCE AND ENGINEERING, XIAN 710072, CHINA

* Corresponding author:limeng@lingnan.edu.cn

powder-forming machine at 300 MPa of pressure. The cemented carbide substrate specimen were prepared by pre-sintering in a tube furnace, and the final sintering was performed in an atmosphere furnace. Firstly, the temperature was increased from room temperature to 400°C at a heating rate of 10°C/min, and the temperature was kept for 1 h, then increased to 600°C and kept for 1 h. The specimens were heated then from 600°C to 900°C at a heating rate of 10°C/min for 0.5 h. Finally, the specimens were heated to 1200°C at a heating rate of 5°C/min and kept for 0.5 h. During the final sintering, the frequency-conversion-constant-pressure-technology was used to heat the specimens to the sintering temperature (1380°C) at a heating rate of 5°C/min in the argon pressure range of 5-200 Pa, and the holding time was 1 h. Finally, as the furnace cools, the specimens needed for the test were obtained. The surface of the specimens was roughly polished, then delicately polished with a diamond polishing disc of 800 mesh to 1500 mesh. Then the specimens were polished to the mirror surface with a metallographic polishing agent of 5.00 μm to 0.25 μm. Finally, they were ultrasonically cleaned with ethanol for 15 min and dried in an oven at 80°C for 120 min until dry. To ensure the consistency of the microtextured morphology, three different pitches of microweave were processed on the substrate surface within 5.00 × 5.00 mm with an automatic scratch tester under a constant load of 80 N. The texture was 4.70 mm long, 100 μm wide, and the spacing from dense to sparse was 500, 750, and 1000 μm, respectively. TiAlCrSiN coating was deposited on the surface of some specimens by multi-arc ion plating technology, and uncoated and coated specimens were obtained. Uncoated specimens were numbered W_1-W_4, and coated specimens were numbered H_1-H_4, where W_1 and H_1 correspond to specimens without microtextured on the surface, respectively.

2.2. Test Method

The surface morphology of the specimen was observed by stereomicroscope and metallographic microscope. The Vickers hardness of the specimens was measured by a Vickers hardness tester. The loading load was 30 kg, the holding pressure was 15 s, and the pressing speed was 0.1 mm·s^{-1}. The average value of 10 points on each specimen was measured. The target source was Co, and XRD (D8 DISCOVER, Bruker) was used to analyze the phase in the specimens. The interface bonding strength between cemented carbide substrate and TiAlCrSiN coating was measured by coating adhesion automatic scratch tester. The loading indenter was a diamond indenter with a 120° cone angle and a 0.2 mm tip radius. The loading load was 60 N, the loading rate was 60 N/min, and the scratch length was 4.0 mm.

3. Results and discussion

3.1. XRD analysis

The XRD patterns of the WC-8Co cemented carbide substrate and TiAlCrSiN coating surface are shown in Fig. 1. The XRD patterns of the WC-8Co substrate mainly presents the (001), (100), (101), (110), and (002) diffraction peaks of WC and the (111) diffraction peak of Co. The XRD patterns of the substrate materials with five kinds of microtextured spacings are consistent, except for the diffraction peak intensity.

The XRD patterns of TiAlCrSiN coating include TiN (111), CrN (200), and AlN (220) diffraction peaks. The TiN diffraction peak shifts to a high angle relative to the diffraction peak in the standard PDF card. This may be due to the formation of TiAlN solid solution by adding Al atoms to replace some Ti atoms in TiN. The radius of the Al atom is smaller than that of the Ti atom, resulting in a smaller interplanar spacing d. The Bragg equation shows that the diffraction peak angle becomes larger and shifts to the right [7]. No evident Si or SiN_X was observed in the figure, indicating that the Si element may exist in the amorphous form in the coating [8].

3.2. Surface morphology

The surface morphology of the specimen before and after the coating deposition is shown in Fig. 2. The surface microtex-

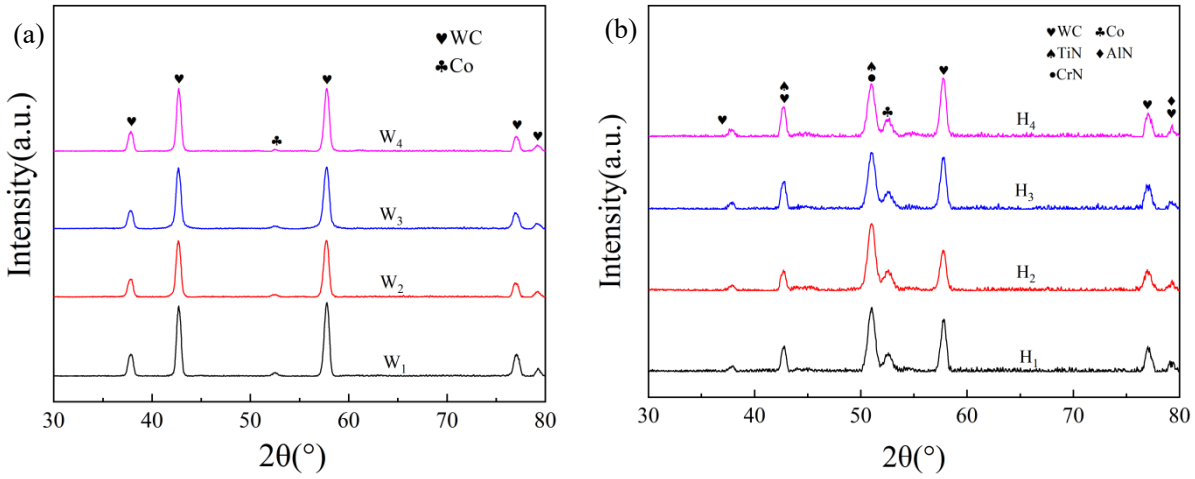

Fig. 1 XRD pattern of cemented carbide substrate and coating: (a) substrate, (b) coating

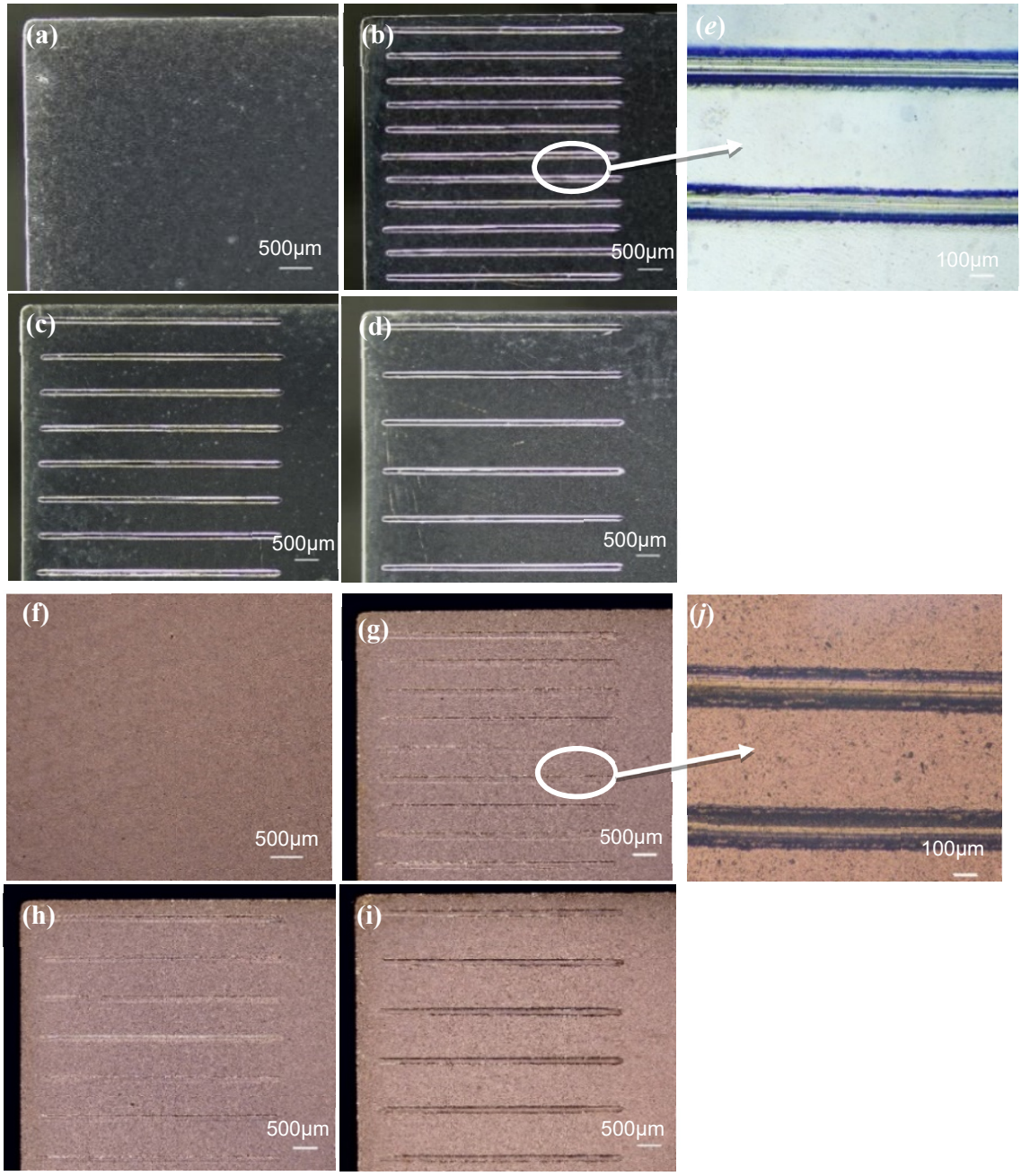

Fig. 2. Surface morphology of the specimen: (a)-(d) W_1-W_4, (f)-(i) H_1-H_4, (e) and (j) are the local enlarged graphs of (b) and (g), respectively

tured morphology of the specimen before depositing the coating is shown in Fig. 2(a)-(d) (corresponding to specimens W_1 to W_4). Panel (a) is the surface morphology of the specimens without microtextured on the surface, and (b)-(d) corresponds to the surface morphology of the specimen with a spacing of 500, 750, and 1 000 μm from dense to sparse, respectively. Panel (e) is the local amplification morphology of the microtextured surface of the specimen with 500 μm spacing corresponding to (b).

The microtextured distribution on the surface of the four specimens is uniform, the grooves are uniform, and the scratch edges are neat, thus ensuring that the microtextured surface morphology prepared by the scratch tester is the same. The groove length of the three microtextures' surface is about 4.70 mm, and the average width of the groove is about 100 μm. The groove spacing meets the requirements of experimental design. The microtextured surface morphology of the specimen after depositing the TiAlCrSiN coating is shown in Fig. 2 (f)-(i), corresponding to the surface morphology of the four coated specimens H_1-H_4, respectively. Fig. 2(f) shows no microtextured on surface morphology of the coated specimen. Fig. 2 (g)-(i) corresponds to the surface morphology of specimens with 500, 750, and 1000 μm spacing, respectively. Fig. 2(j) is the local amplification morphology of the microtextured surface of the coated specimen with 500 μm spacing. The TiAlCrSiN coating deposited on the surface of four cemented carbide substrates by commercial multi-arc ion plating technology is relatively complete, with uniform color and no evident holes or other defects in the coating surface.

3.3. Hardness

The Vickers hardness of the surface of the specimen was tested by a Vickers hardness tester. Ten points were randomly selected on the surface of each specimen. The arithmetic mean of the measured results was used to calculate the indentation fracture toughness using Eq. (1) [9].

$$K_{IC} = 0.0028\sqrt{\frac{HV \times P}{L}} \quad (1)$$

Where HV is Vickers hardness (kg/mm^2), P is applied load (N), and L is the sum of crack length around the hardness indentation (μm).

Fig. 3 shows the Vickers hardness of the specimen. The black and red lines indicate the Vickers hardness of the surface before and after the preparation of the microtextured in the surface of the cemented carbide substrate, respectively.

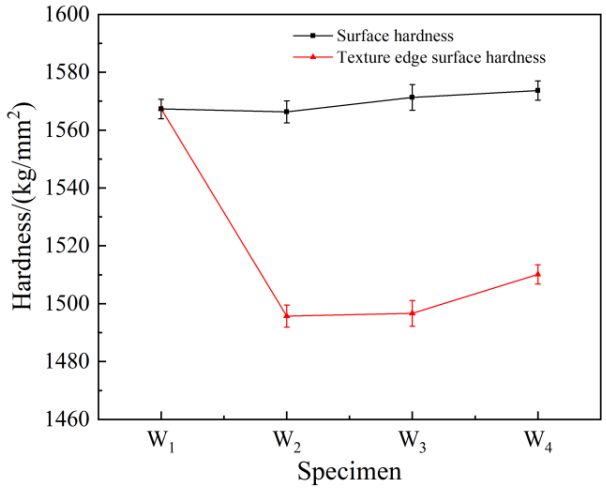

Fig. 3 Vickers hardness of W_1-W_4

The microtextured surface has little effect on the Vickers hardness of the cemented carbide substrate surface. The hardness of the specimen before the microtexture process changes little, distributed in the range of 1567-1573 kg/mm^2. The hardness value is similar to the commercially prepared cemented carbide with the same formula [10]. However, it is slightly smaller than the hardness value of the cemented carbide prepared by hot-pressed sintering [11]. This is mainly due to the difference in the sintering process. To prevent the transition evaporation of the Co phase during high-temperature sintering and enhance the bonding strength of the coating/substrate interface, the cemented carbide substrate specimens were prepared by a high-temperature liquid phase sintering process under an argon pressure of 5-200 Pa by variable frequency constant pressure technology. Then the hard phase multi-element coating was deposited. After obtaining the microtextured surface, the hardness value is in the range of 1496-1510 kg/mm^2, a decrease compared to the hardness without a microtextured surface. The denser the microtextured, the lower the hardness value. This may be attributed to the surface residual stress of the matrix material being released to a certain extent, so slightly decreasing the hardness value [12].

Fig. 4 displays the change in fracture toughness of coated specimens W_1-W_4. The figure's lines represent the fracture toughness change on the specimens' surface. Two small pictures show the surface indentation and sharp corner crack distribution of the W_1 specimen without microtextured coating and the surface indentation and sharp corner crack distribution of the W_2 specimen with a microtextured coating (500 μm spacing). The fracture toughness of the surface of the non-microtextured specimen (W_1) is about 9.71 MPa·m$^{1/2}$. For the specimen with the microtextured surface (W_2-W_3), fracture toughness is 13.42-13.68 MPa·m$^{1/2}$. This result indicates that the microtextured surface effectively improves the fracture toughness of the cemented carbides. As the scratches of the microtextured become sparser, the fracture toughness value decreases slightly, from 13.68 MPa·m$^{1/2}$ (500 μm spacing) to 13.42 MPa·m$^{1/2}$ (1000 μm spacing). This is mainly because the microtextured surface can greatly increase the specimen's specific surface area and surface energy compared with the smooth surface. The closer the scratch, the smaller the spacing. In this case, the specific surface area of the specimen surface is larger, and the surface energy is higher. The increase in specific surface area and surface energy can significantly improve the fracture toughness of the specimen [13,14].

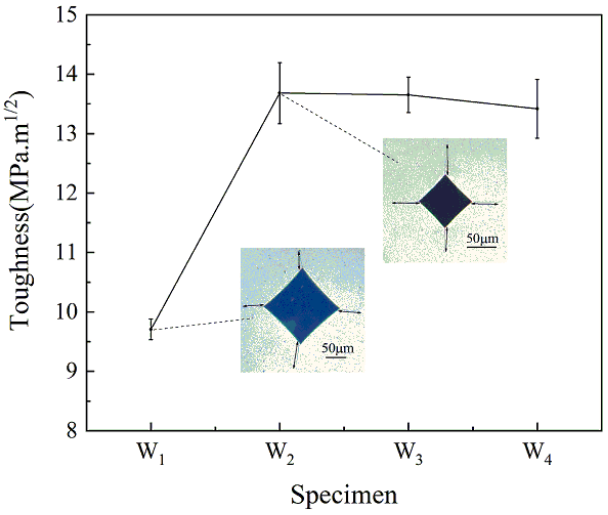

Fig. 4. Fracture toughness of specimens W_1-W_4

3.4. Interfacial bonding strength

The bonding strength between the coating and substrate is an important index to evaluate the coating quality [15]. The bonding strength between the coating and the substrate is affected by many factors [16], such as the substrate composition (WC grain size, Co content), the deposition method, the parameters of the coating, and the pretreatment process of the substrate surface. Among them, roughening treatment such as sandblasting and grinding on the substrate surface or preparing micro-grains (microtexture) on the substrate surface can improve the interfacial bond strength of the substrate/coating system. During loading and

moving the indenter in the coating scratch test, the coating will gradually fracture until it snaps or peels, exposing the substrate. Huang et al. [17] found that the bending direction of the internal crack in the scratch trajectory is the same as the sliding direction. Du et al. [18] showed that the substrate undergoes large deformation during scratching. The scratch indenter concentrates the load on the first half during the sliding process, and the indenter pushes the uplifted coating material. Fig. 5 shows the scratch pattern and its local magnification after the automatic scratch test of coating adhesion on the surface of four coated specimens (H_1-H_4). Fig. 5(a) shows the scratch morphology and the three local position magnification of the coated specimen W_1 without

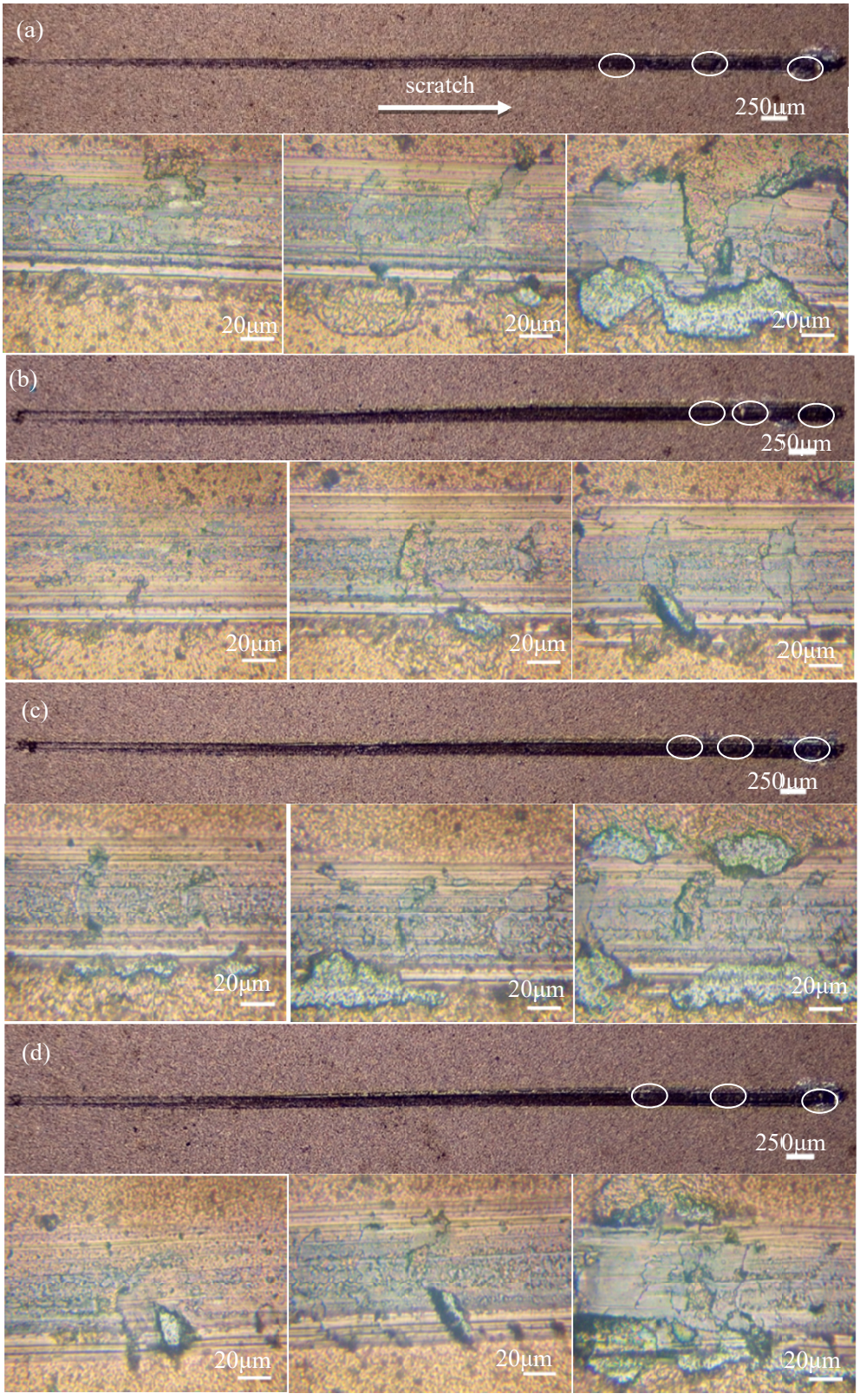

Fig. 5. Surface scratches and local magnification of specimens: (a)-(d) H_1-H_4

a microtextured surface. Fig. 5(b-d) shows the scratch morphology and three local position magnification of the coated specimen W_2-W_4 with 500, 750, and 1000 μm spacing microtextured surface. A location between two scratches was selected for each specimen for the coating adhesion scratch test.

The arrow in Fig. 5 represents the direction of the scratch. The location marked white circle represents the coating's failure and indicates that the cracks started to sprout in the coating along the scratch track. The corresponding load at this time is the critical failure load L_{c1}. Similarly, the critical failure load L_{c2} corresponds to the moment when coating damage is at the edge of the scratch, and the critical failure load L_{c3} corresponds to the partial substrate exposure along the scratch track. The coating on specimen H_1 without a microtextured surface is the first to show cracks, so its corresponding critical failure load L_{c1} is the smallest. After a while, the scratch edge is damaged, and the corresponding critical failure load is L_{c2}. The continuous action of the indenter causes the interface crack propagation or coating fracture of the substrate/coating system. The corresponding critical failure load is L_{c3}, where the coating is severely damaged and peeled off.

Fig. 6 illustrates the acoustic emission (AE) signal diagrams obtained from the scratch test of four different spacing microtextured surface coated specimens, wherein (a)-(d) represent the AE signal diagram of H_1, H_2, H_3, and H_4, respectively. Usually, the scratch load at the time corresponding to the sudden change in position of the AE signal is defined as the coating's critical load value (L_c), which is the critical bonding strength of the coating [2].

The peak value of the AE signal of specimen H_1 is higher than that of specimens H_2-H_4. In general, in the coating scratch test, the lower the peak AE signal intensity of the coating, the higher the toughness of the coating and the lower the hardness under the same experimental conditions. This further verifies that the toughness of H_1 is the lowest, and the hardness is highest. consistent with the changing trend of the previous hardness and fracture toughness experimental data. The peak intensity of the AE signal of specimens with a microtextured surface (H_2-H_4) is lower than that of the specimen without a microtextured surface (H_1). The AE signal peak intensity of the H_2 specimen with 500 μm spacing is the lowest, almost half of the AE signal of the coated specimen without a microtextured surface. In H_3 and H_4 specimens, because the microtexture's spacing increases and the surface scratches become sparse, their toughness values decrease, and their hardness value increase. The surface hardness of the substrate, the surface roughness of the specimen, or the microtextured surface often affect the interfacial bonding strength between the substrate/coating system. The adhesion of the coating can be improved by adjusting the hardness of the substrate's surface or changing the surface roughness of the substrate. However, the microtextured surface significantly influences the interfacial bonding strength between the coating substrate. It is considered that the microtextured surface usually increases the Van der Waals force between the groove

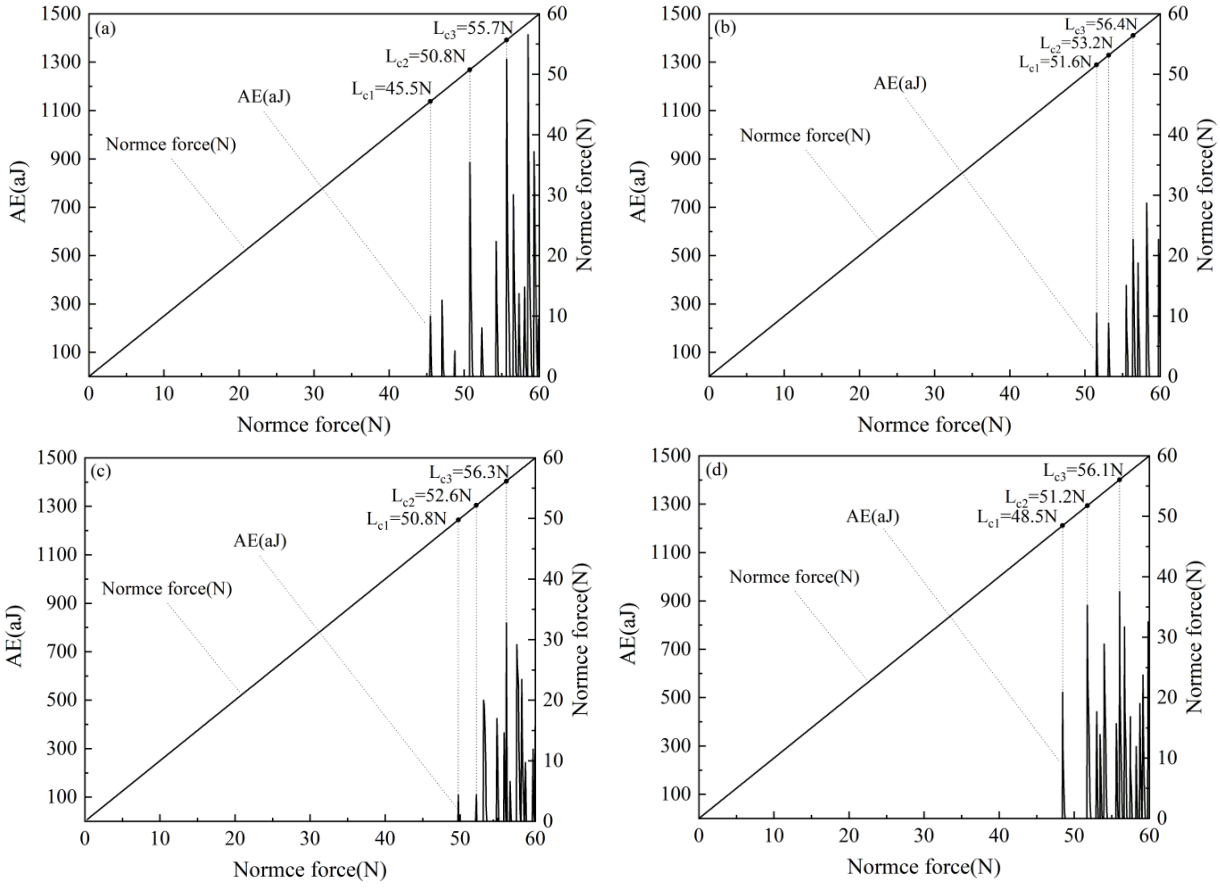

Fig. 6 Acoustic Emission Signal of Scratch Test: (a)-(d) H_1-H_4

and the coating, which improves the mechanical bite between the substrate coating and the mechanical bonding degree, thus increasing the interface bonding strength [23]. Croll et al. [24] pointed out that the surface contact area increased by substrate surface roughening can form more interface bonds in the same area range. It means that the specific surface area and surface energy of the specimen surface are increased, increasing the mechanical bonding strength of the substrate/coating system.

Significantly, the appearance of critical failure load Lc1 corresponding to the specimen (H_2, H_3, and H_4) with the microtextured surface is higher than that of the H1 specimen. Similarly, their values of the failure load L_{c2} of coating damage and L_{c3} of substrate exposure are also higher than that of the H_1 specimen. Compared with other specimens, the L_{c1} corresponding to the crack initiation of the H_2 specimen is the highest, and the coating is less damaged. It is suggested that the microtextured surface effectively improves the bonding strength of the coating interface. Therefore, specimens H_4 and H_2 with a relatively sparse and close spacing have a higher critical force corresponding to the failure time of the coating. The denser the microtexture, the higher the critical failure load for the specimen with microtextured surfaces. Therefore, the coating interface bonding strength of the coated specimen H_2 with 500 μm spacing is the highest, while that of coated specimens H_3 and H_4 with 750 and 1000 μm spacing are lower. The H_1 specimen without a microtextured surface has the lowest interfacial bonding strength. This is mainly due to the treatment of the microtexture surface, which increases the substrate's specific surface area and surface energy, thus improving the adhesion between the coating and the substrate and enhancing the peel and damage resistance of the coated tool [19-21].

TABLE 1 lists the critical failure loads corresponding to the coated specimen H_1 without a microtextured surface; the L_{c1} value is 45.5 N, the L_{c2} is 50.8 N, and the L_{c3} is 55.7 N, respectively. The critical failure loads corresponding to the specimen H_2 with microtextured surface and having 500 μm spacing are the highest; the L_{c1} is 51.6 N, the L_{c2} is 53.2 N, and the L_{c3} is 56.4 N, respectively. The critical failure loads (L_{c1}, L_{c2}, L_{c3}) corresponding to the H_4 specimen with surface microtextured and 1000 μm spacing are 48.5 N, 51.2 N, and 56.1 N, respectively. The critical failure loads (L_{c1}, L_{c2}, L_{c3}) of specimen H_3 with surface microtextured and 750 μm spacing are 50.8 N, 52.6 N, and 56.3 N, respectively. It is concluded that the microtextured surface effectively improves the interfacial bonding strength. The closer spacing of the microtextured surface, the larger the specific surface area of the specimen, the higher the surface energy, and the higher the interfacial bonding strength.

TABLE 1

Failure loads corresponding to damaged H_1-H_4 coatings

Specimen / Failure load/(N)	H_1	H_2	H_3	H_4
L_{C1}	45.5	**51.6**	50.8	48.5
L_{C2}	50.8	**53.2**	52.6	51.2
L_{C3}	55.7	**56.4**	56.3	56.1

4. Conclusions

In this paper, the interface bonding strength of the deposited coating on the substrate surface can be improved by preparing micro-textures with different spacing on the cemented carbide surface. The main conclusions are as follows:

(1) The fracture toughness values of all specimens with microtextured surfaces were higher than that of all specimens without microtextured surfaces. The increase is more evident with the decreasing spacing of the microtextured surface. On the contrary, the Vickers hardness values of all specimens with microtextured surfaces were lower than that of all specimens without microtextured surfaces. With the decreasing spacing of the microtextured surface, the increase is weaker. This indicates that having the microtextured surface can increase the fracture toughness and decrease the Vickers hardness of the WC-8Co cemented carbides.

(2) All microtextured specimens' interfacial bonding strength was higher than those without a microtextured surface. The increasing influence becomes more evident with the decreasing spacing of the microtextured surface. This shows that the microtextured surface can effectively improve the interfacial bonding strength between the coating and the substrate. Usually, the smaller the spacing and the denser the microtexture, the larger the specific surface area of the specimen, and the higher the surface energy and the interfacial bonding strength.

Acknowledgments

This work was supported by the National Natural Science Foundation of China(52005239), Guangdong Provincial Natural Science Foundation of China(2018A030307017) and the Innovative Team in Higher Educational Institutions of Guangdong Province (Natural Science) (Grant No.2020KCXTD039).

REFERENCES

[1] M. Li, Z.L. Song, M.F. Gong, et al., WC+Co+graphene platelet composites with improved mechanical, tribological and thermal properties [J]. Ceramics International **47** (21), 30852-30859 (2021).

[2] M.F. Gong, J. Chen, X. Deng, et al., Sliding wear behavior of TiAlN and AlCrN coatings on a unique cemented carbide substrate [J]. International Journal of Refractory Metals and Hard Materials **69**, 209-214 (2017).

[3] D.H. Xiang, H.R. Feng Z.H. Guo, et al., Preparation technology and properties of microtexture diamond-coated tools [J]. International Journal of Refractory Metals and Hard Materials **76**, 16-24 (2018).

[4] J.T. Wang, X.L. Bai, X.H. Shen, et al., Effect of microtextured on substrate surface on adhesion performance of electroless NiP coating [J]. Journal of Manufacturing Processes **74**, 296-307 (2022).

[5] A.X. Feng, B. Wang, Y. He et al., Study on influence of laser microtextured on bonding properties of cemented carbide TiAlN coating [J]. Hot Working Process **46** (14), 155-158 (2017).

[6] X.H. Zhan, Y.C. Liu, P. Yi, et al., Spreading analysis of plasma spray droplet on sinusoidal textured surfaces [J]. Surfacing **50** (08), 109-121 (2021).

[7] C.H. Liu, J. Li, Z.T. Wu, et al., Preparation and cutting performance of TiAlSiN coatings by pulsed arc ion plating [J]. China Surface Engineering **31** (06), 44-54 (2018).

[8] T.C. Fu, S.J. Yan, C.X. Tian, et al., CrAlTiN and CrAlTiSiN nanocomposite coatings deposited by multi-arc plasma deposition [J]. China Surface Engineering **26** (01), 20-26 (2013).

[9] D.K. Shetty, I.G. Wright, P.N. Mincer, Indentation fracture of WC-Co cermets [J]. Journal of Materials Science **20**, 1873-1882 (1985).

[10] Q.J. Ding, Y. Zheng, Z. Ke, et al., Effects of fine WC particle size on the microstructure and mechanical properties of WC-8Co cemented carbides with dual-scale and dual-morphology WC grains [J]. International Journal of Refractory Metals and Hard Materials **87**, 105166 (2020).

[11] Y.Q. Ye, H.Y. Xia, Y.J. Lin, et al., Refined WC grain size and improved mechanical properties in a hardmetal WC-8Co processed via short-time semi-solid hot pressing [J]. Journal of Alloys and Compounds **889**, 161560 (2021).

[12] Y. He, A.X. Feng, H.X. Zhang, et al., Cemented carbide substrate micro texture and the influence on the bonding properties of the TiAlN coating film-based [J]. Applied Laser **34** (06), 504-507 (2014).

[13] K.D. Zhang, C. Zhang, H.S. Li et al., Study on the substrate surface micro-texturing/carburizing regulating the film-substrate adhesion and wear behavior of DLC coatings [J]. Diamond and Related Materials **130**, 109535 (2022).

[14] Robert O. Ritchie, The conflicts between strength and toughness [J]. Nature Materials **10** (11), 817-822 (2011).

[15] J. Wang, Z.Y. Li, J.S. Luo, et al., Effects of three-dimensional roughness parameters of sandblasted surface on bond strength of thermal spraying coating [J]. Surfacing **48** (05), 246-252+285 (2019).

[16] L.H. Zhu, T. Hu, X. Peng, et al., Effect of al content on adhesion strength of TiAlN coatings [J]. Journal of Material Heat Treatment. **36** (03), 154-158 (2015).

[17] K. Huang, F.L. Yang, L.X. Chen, et al., Study on the adhesion strength of a TiAlN coating by scratch tester [J]. Surface Technology **42** (05), 107-111 (2013).

[18] J. Du, M. Wang H.X. Wang, Analysis of influencing factors on critical load of adhesion strength in scratch test [J]. Surface Technology **44** (09), 134-139 (2015).

[19] J.T. Wang, X.L. Bai, X.H. Shen, et al., Effect of microtextured on substrate surface on adhesion performance of electroless Ni P coating [J]. Journal of Manufacturing Processes **74**, 296-307 (2022).

[20] H. Fu, Y.Y. He, J. Yang, et al., Enhancing adhesion strength of PVD AlCrN coating by novel volcano-shaped microtextures: Experimental study and mechanism insight [J]. Surface & Coatings Technology **445**, 128712 (2022).

[21] Y. Meng, J.X. Deng, J.X. Wu, et al., Improved interfacial adhesion of AlTiN coating by micro-grooves using ultrasonic surface rolling processing [J]. Journal of Materials Processing Technology **304**, 117570 (2022).

[22] D.H. Yu, C.Y. Wang, X.L. Cheng, et al., Microstructure and properties of TiAlSiN coatings prepared by hybrid PVD technology [J]. Thin Solid Films **517** (17), 4950-4955 (2009).

[23] T. Sprute, W. Tillmann, D. Grisales, et al., Influence of substrate pre-treatments on residual stresses and tribo-mechanical properties of TiAlN-based PVD coatings [J]. Surface and Coatings Technology **260**, 369-379 (2014).

[24] S.G. Croll, Surface roughness profile and its effect on coating adhesion and corrosion protection: A review [J]. Progress in Organic Coatings **148**, 105847 (2020).